Smart Structures and Systems, *Vol. 25, No. 6* (*2020*) *679-691*
DOI: https://doi.org/10.12989/sss.2020.25.6.679

Extraction of bridge information based on the double-pass double-vehicle technique

Y. Zhan [1], F.T.K. Au [1] and D. Yang*[2,1]

[1] *Department of Civil Engineering*, *The University of Hong Kong*, *Pokfulam*, *Hong Kong*, *China*
[2] *Department of Civil Engineering*, *Hefei University of Technology*, *Hefei*, *China*

(*Received July 22, 2019, Revised December 4, 2019, Accepted January 10, 2020*)

Abstract. To identify the bridge information from the response of test vehicles passing on it (also known as the indirect approach) has aroused the interest of many researchers thanks to its economy, easy implementation and less disruption to traffic. The surface roughness of bridge remains an obstacle for such method as it contaminates the vehicle response severely and thereby renders many vehicle-response-based bridge identification methods ineffective. This study aims to eliminate such effect with the responses of two different test vehicles. The proposed method can estimate the surface profile of a bridge based on the acceleration data of the vehicles running on the bridge successively, and obtain the normalized contact point response, which proves to be relatively immune to surface roughness. The frequencies and mode shapes of bridge can be further extracted from the normalized contact point acceleration with spectral analysis and Hilbert transform. The effectiveness of the proposed method is verified numerically with a three-span continuous bridge. The influence of measurement noise is also examined.

Keywords: indirect approach; mode shape identification; normalized contact point acceleration; surface roughness

1. Introduction

The phenomenon of vehicle-bridge coupling vibration causes the response of a vehicle passing on a bridge to contain the bridge information. To extract useful bridge information from the vehicle response is known as the indirect approach. Such methods have the advantages of convenience and economy due to less hindrance to traffic and fewer sensors required on the test vehicle as compared to the number of sensors required on a bridge in traditional structural health monitoring system. Many meaningful studies have been carried out and methods have been proposed to identify the bridge frequencies (Yang *et al*. 2004, Lin and Yang 2005, Yang and Chang 2009), damping (González *et al*. 2012, Keenahan *et al*. 2014, Yang *et al*. 2019) and mode shapes (Oshima *et al*. 2014, Malekjafarian and Obrien 2017), to locate damage (Bu *et al*. 2006, Zhang, *et al*. 2012, He *et al*. 2014, Li and Au 2014, O'Brien and Keenahan 2015) and to assess the bridge condition (Kim *et al*. 2014). Two reviews of the works in this field are available (Malekjafarian *et al*. 2015, Yang and Yang 2017). This indirect approach can now be used by engineers for bridge monitoring on a regular and routine basis (Yang *et al*. 2019).

The surface roughness severely contaminates the measured vehicle response and masks the components that are related to the bridge vibration. Therefore, it is a major impediment for the indirect approach to go from theory to application. The adverse effect of surface roughness has been pointed out and discussed by various researchers, such as Elhattab *et al*. (2016), and Qi and Au (2016). Most previous studies have assumed the bridge to have smooth surface or considered it but with an impractically small magnitude. A lot of efforts have been made to overcome such an obstacle. Yang *et al*. (2012) employed two connected vehicles to mitigate the blurring effect of road surface roughness in bridge frequency identification. Oshima *et al*. (2014) developed a monitoring system composed of more than four monitoring vehicles and two heavy trucks to estimate the bridge mode shapes and assess the bridge condition. O'Brien *et al*. (2014) composed an algorithm to derive the dynamic vehicle-bridge interaction forces from the vehicle response, based on which the global bending stiffness and roughness profile of the bridge can be identified. However, the multi-vehicle system is expected to encounter difficulties in real applications as the assumptions in simulation can hardly be met in reality for such a complicated system.

This paper addresses this problem by obtaining an estimation of surface profile from the acceleration of two different test vehicles traversing the bridge successively. The normalized contact point acceleration (NCPA) is then obtained, which is relatively immune to the influence of surface roughness. The bridge information such as frequencies and mode shapes can then be identified from the NCPA accordingly.

There exist several methods to detect the surface profile. Nowadays the highway authorities usually resort to the use of road surface profiler, which is essentially a vehicle with laser sensors to record the distance between the road surface and the receiver, and accelerometers to record and

*Corresponding author, Associate Professor,
E-mail: yangdong@hfut.edu.cn

http://www.techno-press.org/?journal=sss&subpage=7
ISSN: 1738-1584 (Print), 1738-1991 (Online)

compensate for the body movement. It provides accurate estimation of surface profile, but there are also obvious shortcomings: expensive to purchase, time-consuming, strict operation condition requirements and high maintenance costs. In addition, the identified surface profile can be quite different from what the vehicle experiences due to the stiffness of tyre and width of the wheel (Captain *et al*. 1979, Chang *et al*. 2011, Camara *et al*. 2014). Fig. 1 shows their difference due to width of the wheel. To eliminate the influence of surface roughness on vehicle response, the experienced, rather than the exact surface profile, is needed. In this study, the experienced surface roughness is identified based on the response of the vehicle entirely.

To study the surface roughness from the vehicle point of view, a vehicle-bridge contact model should be adopted. A widely used model assumes the wheel of the vehicle to remain in contact with the bridge surface, which can be expressed as

$$u_c(t) = u_b(x,t)|_{x=vt} + R(x)|_{x=vt} \tag{1}$$

where $u_c(t)$, $u_b(x,t)|_{x=vt}$ and $R(x)|_{x=vt}$ are the vertical contact point displacement of the vehicle, the vertical contact point displacement of the bridge and the surface roughness at the contact point, respectively. It remains valid as long as the vehicle speed is not very high (Cheng *et al*. 1999). This model is adopted in this study unless otherwise stated.

Once the experienced surface roughness is estimated, its adverse effect on the vehicle response can be eliminated, and the bridge frequencies and mode shapes can be obtained.

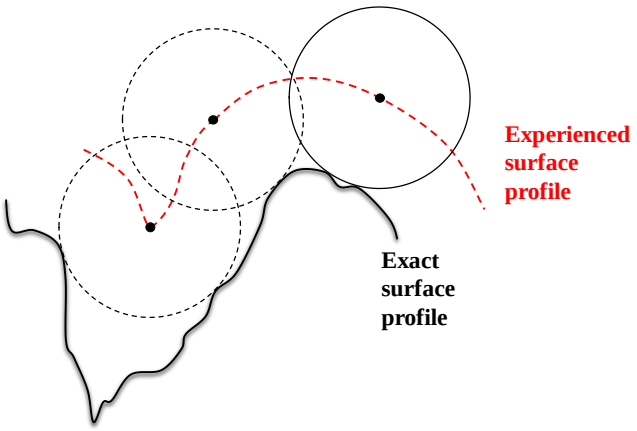

Fig. 1 Difference between exact and experienced surface profiles due to the width of wheel

Consequently, model calibration, updating and damage location can be carried out based on the mode shapes acquired (Brownjohn *et al*. 2001, Chrysostomou and Stassis 2008, Altunisik *et al*. 2012). The pioneering work of constructing the mode shapes of a bridge using the acceleration data of a passing-by vehicle and Hilbert transform has been proposed by Yang *et al*. (2014). Later the work has been extended to the use of contact point responses instead of vehicle response (Yang *et al*. 2018). As the surface roughness may lead to errors in mode shape identification, this study adopts the NCPA obtained from the double-pass double-vehicle (2P2V) technique to overcome the surface roughness problem.

2. Identification of experienced surface roughness

In this section, the theoretical derivation of the spring-mass vehicle model to detect surface roughness is presented. The results are also provided when the bridge damping is considered.

2.1 Theoretical derivation

The governing equations of the vehicle-bridge interaction (VBI) systems shown in Fig. 2 are as follows

$$\bar{m}\frac{\partial^2 u_b(x,t)}{\partial t^2} + EI\frac{\partial^4 u_b(x,t)}{\partial x^4} = f_c(t)\delta(x-vt) \tag{2}$$

$$m_v\frac{d^2 u_v(t)}{dt^2} = k_v[u_b(x,t)|_{x=vt} + R(x)|_{x=vt} - u_v(t)] \tag{3}$$

$$f_c(t) = k_v\{u_v(t) - [u_b(x,t)|_{x=vt} + R(x)|_{x=vt}]\} - m_v g \tag{4}$$

where $\bar{m}$, E and I are the mass per unit length, modulus of elasticity and moment of inertia of the bridge, respectively; m_v and k_v denote the mass and stiffness of the vehicle, respectively; $u_b(x,t)$ is the vertical displacement of the bridge at location x and time t; $u_v(t)$ is the vertical displacement of the vehicle; $f_c(t)$ is the contact force between the bridge and vehicle; $R(x)|_{x=vt}$ is the surface roughness at the contact point, $\delta(x)$ is the Dirac Delta function, and $\delta(x-vt)$ describes the movement of a unit point load at speed v.

From Eq. (2), the displacement of the contact point of the bridge can be derived by mode superposition method (Clough and Penzien 2003). The vertical displacement of the bridge can be expressed as

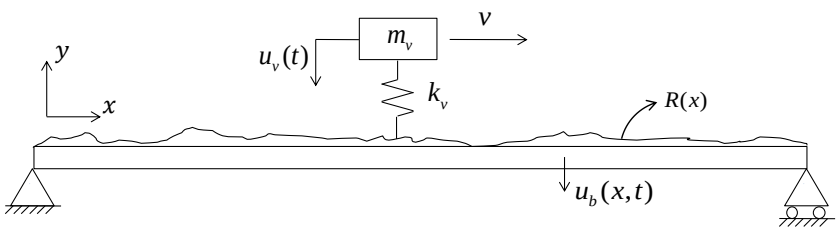

Fig. 2 Illustration of the vehicle-bridge interaction system

$$u_b(x,t) = \sum_{i=1}^{\infty} \left[\phi_i(x) \cdot Y_i(t)\right] \tag{5}$$

where $\phi_i(x) = \sin\frac{i\pi x}{L}$ is the *i*-th mode shape of the bridge, and $Y_i(t)$ is the associated modal amplitude.

Assuming that the vehicle mass is negligibly small compared to the bridge mass, the modal amplitude can be solved as (Zhan and Au 2019)

$$Y_j(t) = \frac{-2(m_v g + k_v R(x)|_{x=vt})L^3}{j^4\pi^4 EI - j^2\pi^2 v^2 L^2 \bar{m}} \left[\sin\frac{j\pi vt}{L} - \frac{j\pi v}{L\omega_{bj}}\sin(\omega_{bj}t)\right] \tag{6}$$

where $\omega_{bj} = \frac{j^2\pi^2}{L^2}\sqrt{\frac{EI}{\bar{m}}}$ is the *j*-th circular frequency of the bridge.

Substituting Eq. (6) back into Eq. (5), the displacement of the bridge at the contact point is obtained as

$$u_b(x,t)|_{x=vt} = \sum_{j=1}^{\infty} \frac{-2(m_v g + k_v R(x)|_{x=vt})L^3}{j^4\pi^4 EI - j^2\pi^2 v^2 L^2 \bar{m}} \sin\frac{j\pi vt}{L} \left[\sin\frac{j\pi vt}{L} - \frac{j\pi v}{L\omega_{bj}}\sin(\omega_{bj}t)\right] \tag{7}$$

The contact point responses of the vehicle can be derived from Eq. (3). By a simple rearrangement of the terms, the displacement and acceleration of the contact point are obtained, respectively, as

$$u_c(t) = \frac{1}{\omega_v^2}a_v(t) + u_v(t) \tag{8}$$

$$a_c(t) = \frac{1}{\omega_v^2}\frac{d^2 a_v(t)}{dt^2} + a_v(t) \tag{9}$$

where $\omega_v = \sqrt{k_v/m_v}$ denotes the circular frequency of the vehicle. With an accelerometer installed on the chassis, the vehicle acceleration $a_v(t)$ is recorded. By numerical integration with zero initial condition, the displacement of the vehicle $u_v(t)$ can be obtained. The acceleration history and the vehicle frequency are both the required information for using the proposed method.

The contact point displacement of the vehicle can be written as

$$u_c(t) = [m_v g + k_v R(x)|_{x=vt}]\bar{u}(t) + R(x)|_{x=vt} \tag{10}$$

where $\bar{u}(t) = \sum_{j=1}^{\infty} \frac{-2L^3}{j^4\pi^4 EI - j^2\pi^2 v^2 L^2 \bar{m}} \sin\frac{j\pi vt}{L}\left[\sin\frac{j\pi vt}{L} - \frac{j\pi v}{L\omega_{bj}}\sin(\omega_{bj}t)\right]$ is the normalized contact point displacement of the bridge, which is the response at the contact point of the bridge under a unit load travelling at the speed v, and is dependent on the bridge properties such as span length, stiffness and circular frequency. However, the vehicle properties are not involved except for the vehicle speed v.

Note that Eq. (10) contains two unknowns $\bar{u}(t)$ and $R(x)|_{x=vt}$, which requires two more equations to solve. Consequently, a 2P2V technique is proposed to estimate the surface profile:

Step 1: Let the first vehicle of frequency ω_{v1} pass over the bridge at a constant speed v and record its vertical acceleration history $a_1(t)$.

Step 2: Let the second vehicle of frequency ω_{v2} pass over the bridge at the same speed v and record its vertical acceleration history $a_2(t)$.

Step 3: Calculate the contact point displacements $u_{c1}(t)$ and $u_{c2}(t)$ with Eq. (8).

Completing the above mentioned three steps, an equation set can be obtained as

$$\begin{aligned}&[m_{v,n}g + k_{v,n}R(x)|_{x=vt}]\bar{u}(t) + R(x)|_{x=vt} \\ &= u_{c,n}(t), \qquad n = 1,2\end{aligned} \tag{11}$$

where the subscript *n* denotes the first and second passes. Combining the equation set to get a quadratic equation in terms of $R(x)|_{x=vt}$, the solution can be obtained as

$$R_{1,2} = \frac{-b \pm \sqrt{b^2 - 4ac}}{2a} \tag{12}$$

where $a = \beta\omega_{v2}^2 - \omega_{v1}^2$, $b = (\beta-1)g + \omega_{v1}^2 u_{c2}(t) - \beta\omega_{v2}^2 u_{c1}(t)$, $c = g[u_{c2}(t) - \beta u_{c1}(t)]$, and β denotes the mass ratio of the two vehicles, i.e., $\beta = m_{v2}/m_{v1}$. $R_{1,2}$ denotes the possible roots of $R(x)|_{x=vt}$ at a certain instant t. To determine which one is the desired solution, one may analyse Eq. (12) first by looking into a simple case where the two vehicles are of the same frequency, i.e., $\omega_{v1} = \omega_{v2} = \omega_v$. In this case, one has

$$R_{1,2} = \frac{-\left[(\beta-1)g + \omega_v^2\left(u_{c2}(t) - \beta u_{c1}(t)\right)\right] \pm |(\beta-1)g - \omega_v^2[u_{c2}(t) - \beta u_{c1}(t)]|}{2(\beta-1)\omega_v^2} \tag{13}$$

If $(\beta-1)g - \omega_v^2[u_{c2}(t) - \beta u_{c1}(t)] \geq 0$, then $R_1 = \left(u_{c2} - \beta u_{c1}(t)\right)/(1-\beta)$ and $R_2 = -g/\omega_v^2$. R_2 is a constant but the surface roughness is obviously a variable, leaving behind R_1 as the desired solution. Similarly, if $(\beta-1)g - \omega_v^2[u_{c2}(t) - \beta u_{c1}(t)] < 0$, then $R_1 = -g/\omega_v^2$ and $R_2 = \left(u_{c2} - \beta u_{c1}(t)\right)/(1-\beta)$, which gives R_2 as the desired solution. In either case, one has $R = \left(u_{c2} - \beta u_{c1}(t)\right)/(1-\beta)$.

In the general case where ω_{v1} may not be equal to ω_{v2}, one can rearrange and regroup the terms of Eq. (12) to get

$$R_{1,2} = \frac{-b \pm \sqrt{p^2 - q}}{2a} \tag{14}$$

where $p = (\beta-1)g - \omega_{v1}^2 u_{c2}(t) + \beta\omega_{v2}^2 u_{c1}(t)$ and $q = 4g\beta(\omega_{v2}^2 - \omega_{v1}^2)[u_{c2}(t) - u_{c1}(t)]$. Eq. (14) is still complicated for analysis, but q has little effect on the final solution, as it is negligible compare to p^2. To demonstrate this, simulations have been conducted to examine the ratio

$\lambda = \frac{q}{p^2}$ with different values of β, ω_{v1}, ω_{v2} and surface roughness classes.

To cover the normal frequency range of vehicle, the simulation ranges of ω_{v1} and ω_{v2} are set to be 0.4 ~ 2.2 Hz, with an interval of 0.1 Hz (Gillespie 1997). The mass ratio β is within the range of $2^{0.25}$ to 2^2, with exponential increments of 0.25. The cases of smooth surface and 5 classes of rough surface from Class A (very good) to Class E (very poor) as defined by ISO (2016) are considered in the simulation.

The results of all the simulations indicate that λ is very small in most of the cases. In fact, there is 96.9% chance for having $\lambda < 5\%$. To provide visual indication, the results of λ under smooth surface and Class C (average quality) surface conditions are presented in Figs. 3 and 4, respectively, whose horizontal and vertical axes denote the frequencies of two vehicles, ranging from 0.4 to 2.2 Hz.

Since λ is small in most of the cases, q can be neglected, and a similar approach for the case of same vehicle frequency can be adopted. If $p \geq 0$, one has $R_{1a} = -\frac{\omega_{v1}^2 u_{c2}(t) - \beta\omega_{v2}^2 u_{c1}(t)}{\beta\omega_{v2}^2 - \omega_{v1}^2}$ and $R_{2a} = -\frac{(\beta-1)g}{\beta\omega_{v2}^2 - \omega_{v1}^2}$. Since R_{2a} is a constant, R_{1a} is the desired solution; otherwise if $p < 0$, $R_{2a} = -\frac{\omega_{v1}^2 u_{c2}(t) - \beta\omega_{v2}^2 u_{c1}(t)}{\beta\omega_{v2}^2 - \omega_{v1}^2}$ is the desired solution. Since q has little effect on the final solution, the exact solutions $R_1(t)$ and $R_2(t)$ differ little from their approximations R_{1a} and R_{2a}, respectively, which means that either one of $R_1(t)$ and $R_2(t)$ is nearly constant and therefore it cannot be the desired solution. This offers a criterion for choosing the desired solution: the one that differs more from $-\frac{(\beta-1)g}{\beta\omega_{v2}^2 - \omega_{v1}^2}$ is the desired solution.

Therefore, a method for calculating the surface roughness R using vehicles with different frequencies is proposed. For every time instant, calculate R_1 and R_2 according to Eq. (14). The solution that differs more from the constant $-\frac{(\beta-1)g}{\beta\omega_{v2}^2 - \omega_{v1}^2}$ is the desired solution. The process can be expressed in pseudocode as: if $\left|R_1 + \frac{(\beta-1)g}{\beta\omega_{v2}^2 - \omega_{v1}^2}\right| \geq \left|R_2 + \frac{(\beta-1)g}{\beta\omega_{v2}^2 - \omega_{v1}^2}\right|$, then R_1 is the desired solution; otherwise R_2 is the desired solution.

Note that neglecting q only occurs in the solution selection procedures but not in the solution process itself.

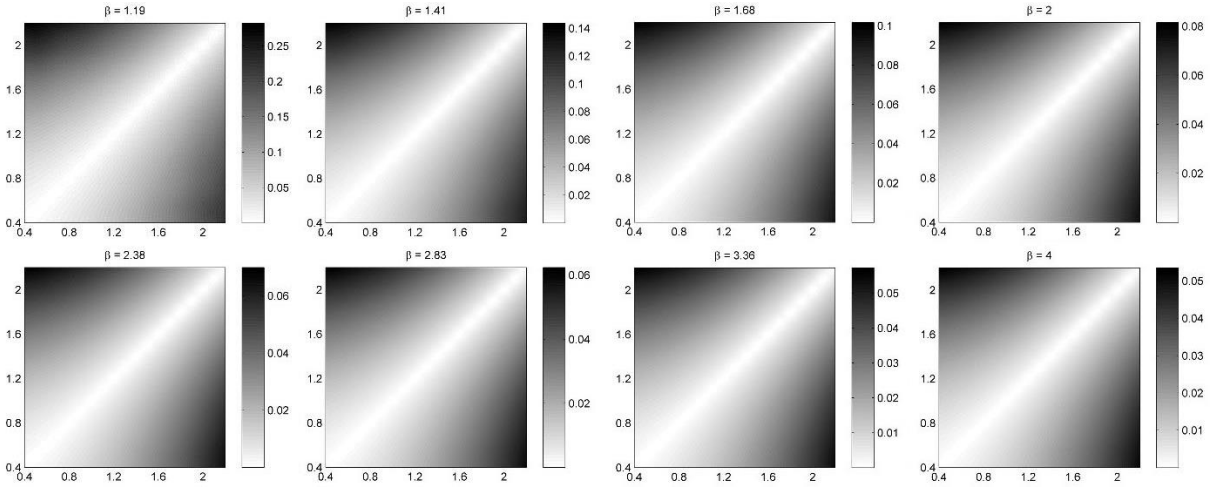

Fig. 3 λ under smooth surface condition

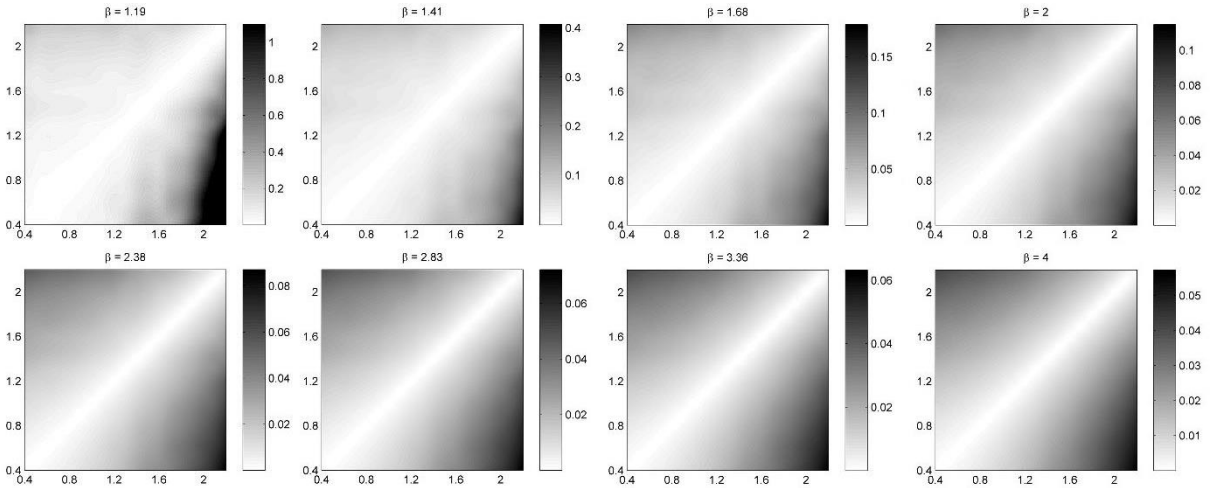

Fig. 4 λ under Class C (average quality) surface condition

The calculation of R_1 and R_2 does not involve approximation and hence the value of R is accurate.

For an extreme case where $q > p^2$, complex solutions would occur. This happens when ω_{v2} is much larger or smaller than ω_{v1} and β is close to 1, which means that the two vehicles are very close in mass but quite different in stiffness. This rarely happens and it can be avoided by carefully selecting the test vehicles. Nonetheless, if a complex number occurs, one could still get a fair estimation of the surface roughness by the approximation $R = -\frac{\omega_{v1}^2 u_{c2}(t) - \beta\omega_{v2}^2 u_{c1}(t)}{\beta\omega_{v2}^2 - \omega_{v1}^2}$.

2.2 Theoretical results considering bridge damping

When the bridge damping is considered, Eq. (2) becomes

$$\bar{m}\frac{\partial^2 u_b(x,t)}{\partial t^2} + c\frac{\partial u_b(x,t)}{\partial t} + EI\frac{\partial^4 u_b(x,t)}{\partial x^4} = f_c(t)\delta(x - vt) \tag{15}$$

where c denotes the damping coefficient of the bridge. The displacement of the bridge at the contact point ignoring the transient response is obtained as

$$u_b(x,t)|_{x=vt} = \frac{-2(m_v g + k_v R(x)|_{x=vt})L^3}{j^4\pi^4 EI\left[\left(1-\beta_j^2\right)^2 + \left(2\xi_{bj}\beta_j\right)^2\right]} \sum_{j=1}^{\infty} \sin\frac{j\pi vt}{L}\left[\left(1-\beta_j^2\right)\sin\frac{j\pi vt}{L} - 2\xi_{bj}\beta_j\cos\frac{j\pi vt}{L}\right] \tag{16}$$

where $\omega_{bjd} = \omega_{bj}\sqrt{1-\xi_{bj}^2}$ is the j-th damped frequency of the bridge, and $\beta_j = \frac{j\pi v}{L\omega_{bj}}$ is the ratio of the loading frequency to the j-th structural frequency.

Following the same process, one can derive the surface roughness. The difference lies in that the normalized contact point displacement of the bridge becomes $\bar{u}(t) = \sum_{j=1}^{\infty}\frac{-2L^3}{j^4\pi^4 EI\left[\left(1-\beta_j^2\right)^2+\left(2\xi_{bj}\beta_j\right)^2\right]}\sin\frac{j\pi vt}{L}\left[\left(1-\beta_j^2\right)\sin\frac{j\pi vt}{L} - 2\xi_{bj}\beta_j\cos\frac{j\pi vt}{L}\right]$ when bridge damping is considered.

3. Extraction of bridge frequencies and mode shapes

The normalized bridge contact point displacement $\bar{u}(t)$ is in theory free of the surface roughness contamination. $\bar{u}(t)$ can be determined following the same procedure as the estimation of surface profile R in Section 2. Using trigonometric identities, $\bar{u}(t)$ can be rewritten as

$$\bar{u}(t) = \sum_{j=1}^{\infty}\frac{-L^3}{j^4\pi^4 EI - j^2\pi^2 v^2 L^2\bar{m}} \times\left[1 - \cos\frac{2j\pi vt}{L} + \frac{j\pi v}{L\omega_{bj}}\cos\left(\omega_{bj} + \frac{j\pi v}{L}\right)t - \frac{j\pi v}{L\omega_{bj}}\cos\left(\omega_{bj} - \frac{j\pi v}{L}\right)t\right] \tag{17}$$

Differentiating $\bar{u}(t)$ twice, one obtains the normalized contact point acceleration (NCPA) of the bridge $\bar{a}(t)$ as

$$\bar{a}(t) = \sum_{j=1}^{\infty}\frac{-L^3}{j^4\pi^4 EI - j^2\pi^2 v^2 L^2\bar{m}} \times\left[\left(\frac{2j\pi v}{L}\right)^2\cos\frac{2j\pi vt}{L} - \frac{j\pi v}{L\omega_{bj}}\left(\omega_{bj} + \frac{j\pi v}{L}\right)^2\cos\left(\omega_{bj} + \frac{j\pi v}{L}\right)t + \frac{j\pi v}{L\omega_{bj}}\left(\omega_{bj} - \frac{j\pi v}{L}\right)^2\cos\left(\omega_{bj} - \frac{j\pi v}{L}\right)t\right] \tag{18}$$

The NCPA $\bar{a}(t)$ is also free of the surface roughness contamination, but it contains the bridge properties, which makes it possible to extract the bridge frequencies and mode shapes even in the presence of surface roughness. The component response corresponding to the bridge frequency of the j-th mode can be obtained by a suitable filter. The decomposed bridge component response $a_j(t)$ associated with the j-th mode is

$$a_j(t) = A_r\cos\left(\omega_{bj} + \frac{j\pi v}{L}\right)t + A_l\cos\left(\omega_{bj} - \frac{j\pi v}{L}\right)t \tag{19}$$

where $\mathrm{A}_r = \frac{L^3}{j^4\pi^4 EI - j^2\pi^2 v^2 L^2\bar{m}}\frac{j\pi v}{L\omega_{bj}}\left(\omega_{bj} + \frac{j\pi v}{L}\right)^2$ and $\mathrm{A}_l = -\frac{L^3}{j^4\pi^4 EI - j^2\pi^2 v^2 L^2\bar{m}}\frac{j\pi v}{L\omega_{bj}}\left(\omega_{bj} - \frac{j\pi v}{L}\right)^2$.

The Hilbert transform is a linear operator that takes a time series $\mu(t)$ and produces its transform $\hat{\mu}(t)$ as

$$\hat{\mu}(t) = \frac{1}{\pi t}\,\mathrm{p.v.}\int_{-\infty}^{+\infty}\frac{\mu(\tau)}{t-\tau}d\tau \tag{20}$$

where p.v. denotes the Cauchy principal value. Because $(\pi t)^{-1}$ is not integrable, the convolution does not converge, and therefore the Cauchy principal value is adopted to avoid singularities. It is noted that Hilbert transform only applies to narrow band signal and $a_j(t)$ meets such requirement. Therefore, performing the Hilbert transform on $a_j(t)$ gives its transform $\hat{a}_j(t)$

$$\hat{a}_j(t) = A_r\sin\left(\omega_{bj} + \frac{j\pi v}{L}\right)t + A_l\sin\left(\omega_{bj} - \frac{j\pi v}{L}\right)t \tag{21}$$

The instantaneous amplitude (envelope) is defined as the modulus of the transform pairs

$$A_j(t) = \sqrt{a_j^2(t) + \hat{a}_j^2(t)} = \sqrt{(A_r + A_l)^2 - 4A_rA_l\sin^2\frac{j\pi v}{L}t} \tag{22}$$

For the lower modes (e.g., $j \leq 3$), the driving frequency $j\pi vt/L$ is often much smaller than the bridge frequency ω_{bj}, indicating that A_r and A_l are similar in magnitude but opposite in sign. Since the lower modes contain most of the energy, they are sufficient for general engineering purpose. Therefore, Eq. (22) can be approximated as

$$A_j(t) = \sqrt{-4A_rA_l}\left|\sin\frac{j\pi v}{L}t\right| \tag{23}$$

The modulus $A_j(t)$ is the bridge mode shape $\sin(j\pi x/L)$ scaled and given in absolute value. Therefore, it is feasible to use the NCPA to get the bridge mode shape. Consequently, the 2P2V technique is proposed to extract bridge mode shape, and the subsequent steps following those listed in Section 2.1 are:

Step 4: Analyse the NCPA $\bar{a}(t)$ to identify the frequency peaks related to the bridge frequencies using spectral analysis tools.

Step 5: Filter $\bar{a}(t)$ to distil the component acceleration $a_j(t)$ that are associated with the identified bridge frequencies.

Step 6: Calculate $A_j(t)$, the envelope of $a_j(t)$ with Hilbert transform; adjust the sign of $A_j(t)$; and normalize it to get the mode shapes of bridge.

The process of obtaining the surface profile and mode shapes from the vehicle responses are presented in Fig. 5.

4. Numerical verification

In this section, the proposed method is verified numerically using a three-span continuous beam. The influence of measurement noise is also investigated.

4.1 Generation of surface profiles and performance evaluation indices

The surface profiles used in the simulation are generated according to the ISO standard, which classifies surface profiles into Classes A, B, C, D and E, from very good to very poor, respectively, based on their power spectral density (Oliva *et al*. 2013, ISO 2016). A total of 50 surface profiles, with 10 samples in each roughness class, have been generated to test the performance of the method.

To evaluate the performance of the proposed method in the estimation of bridge surface profiles, two performance evaluation indices are introduced. The first one adopts the concept of standard deviation as

$$\sigma = \left[\frac{1}{n}\sum_{i=1}^{n}\left(R_{d,i} - R_{r,i}\right)^2\right]^{1/2} \tag{24}$$

where $R_{d,i}$ denotes the *i*-th element of the identified surface profile sequence and $R_{r,i}$ denotes the corresponding real value. The lower σ is, the better the detection result is. If the identified profile matches the real profile exactly, one has $\sigma = 0$.

Another indicator is the relative area difference (RAD) which is the ratio of the area sandwiched between the detected and real profiles (i.e., the area of error) to the area covered by the real profile, i.e.

$$\text{RAD} = \frac{\int|R_d(x) - R_r(x)|dx}{\int|R_r(x)|\,dx} = \frac{\sum_i\left|R_{d,i} - R_{r,i}\right|\Delta x}{\sum_i\left|R_{r,i}\right|\Delta x} \tag{25}$$

where Δx denotes the spatial sampling interval. The idea behind RAD is that if the profile is substantially uneven, the tolerance of error should be larger compare to a profile that

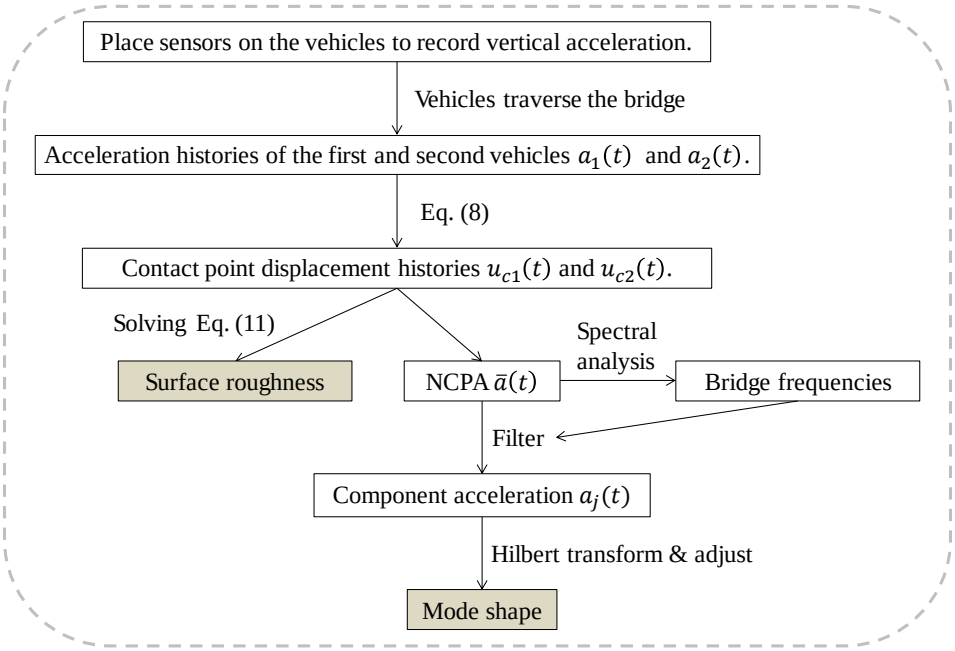

Fig. 5 Flowchart to describe the proposed method

is much smoother, because the same amount of error will cause a larger effect on the latter than the former. This index reflects the relative error compared to the variation of the data set.

The constructed mode shapes are evaluated by the modal assurance criteria (MAC) defined as

$$\mathrm{MAC} = \frac{\varphi_e^T \varphi_t}{|\varphi_e||\varphi_t|} \tag{26}$$

where φ_e is the extracted mode shape and φ_t is the theoretical mode shape and $\mathrm{MAC} \in [0, 1]$. The higher the value of MAC is, the better the detection performance is.

4.2 Finite element formulation

The finite element formulation of the vehicle-bridge interaction system is expressed as

$$\begin{bmatrix} \boldsymbol{M}_b & \boldsymbol{M}_v\boldsymbol{H}(t) \\ \boldsymbol{0} & \boldsymbol{M}_v \end{bmatrix} \begin{Bmatrix} \boldsymbol{a}_b(t) \\ \boldsymbol{a}_v(t) \end{Bmatrix} + \begin{bmatrix} \boldsymbol{C}_b & \boldsymbol{0} \\ -\boldsymbol{C}_v\boldsymbol{H}'(t) & \boldsymbol{C}_v \end{bmatrix} \begin{Bmatrix} \boldsymbol{v}_b(t) \\ \boldsymbol{v}_v(t) \end{Bmatrix} + \begin{bmatrix} \boldsymbol{K}_b & \boldsymbol{0} \\ -\boldsymbol{K}_v\boldsymbol{H}'(t) - v\boldsymbol{C}_v\dot{\boldsymbol{H}}'(t) & \boldsymbol{K}_v \end{bmatrix} \begin{Bmatrix} \boldsymbol{u}_b(t) \\ \boldsymbol{u}_v(t) \end{Bmatrix} = \begin{Bmatrix} -g\boldsymbol{M}_v\boldsymbol{H}(t) \\ \boldsymbol{C}_v\dot{r}(t) + \boldsymbol{K}_v r(t) \end{Bmatrix} \tag{27}$$

where $\boldsymbol{M}$, $\boldsymbol{C}$ and $\boldsymbol{K}$ denote the mass, damping and stiffness matrices, respectively; $\boldsymbol{a}$, $\boldsymbol{v}$ and $\boldsymbol{u}$ denote the acceleration, velocity and displacement vectors, respectively; and the subscripts b and v denote the bridge and the vehicle, respectively; $r(t)$ denotes the surface profile; $\boldsymbol{H}(t)$ is the location vector of the vehicle, whose elements corresponding to the current location of the vehicle are equal to the values of Hermite interpolation vectors shown as $[1-3(x/L)^2+2(x/L)^3 \quad x(1-x/L)^2 \quad 3(x/L)^2-2(x/L)^3 \quad x^2(x/L-1)/L]^T$, with the ratio of abscissa to element length x/L depending on the relative position of the vehicle on bridge, and the rest of the elements are all zeros. Eq. (27) can be solved iteratively with Newmark-β method.

4.3 Simulation results and discussion

The proposed method is applied to a three-span continuous bridge with the following parameters: span lengths 20 + 30 + 20 m, moment of inertia 0.36 m^4, mass per unit length 2000 kg/m, and modulus of elasticity 3.15×10^4 MPa. The data sampling frequency is set at 1000 Hz, i.e., time interval of 0.001 second.

The test vehicles are represented by spring-mass models for simplicity. Two sets of simulations are carried out, including the case of vehicles having the same frequencies and the case with different frequencies. The vehicle parameters are shown in Table 1.

The surface roughness identification results are shown in Table 2. Two phenomena can be observed from the simulation. First, the more uneven the surface profile is, the higher the absolute detection error is, as reflected by an increasing value of σ from Class A to Class E. The relative error is however not the case, as RAD remains at similar magnitude as the surface quality becomes poorer, which means that this method can provide reasonably accurate results even for very poor bridge surface profile. Second, if the two vehicles are of the same frequencies, the detection error is much smaller than that when they are different. Nevertheless, the detection accuracy is acceptable for engineering applications in both cases.

To provide visual indication of the detection accuracy, the identified profile, real profile and identification error of a Class C surface profile are presented in Fig. 6.

Once the surface profile has been estimated, the normalized contact point displacement $\bar{u}(t)$ can be derived using Eq. (11). The NCPA can be obtained accordingly by numerical differentiation. To demonstrate the effects of the surface roughness on the NCPA and the vehicle acceleration, both of them are worked out for the case of the bridge with smooth surface and that with Class C surface.

Table 1 Parameters of test vehicles

Case	Vehicle no.	Mass (kg)	Stiffness (N×m^{-1})	Frequency (Hz)	Speed (m/s)
Same frequencies	1	2000	154755	1.4	2
	2	3000	232133		
Different frequencies	1	2000	154755	1.4	2
	2	3000	170547	1.0	

Table 2 Surface roughness detection results

Case	Error indicator	Surface roughness classes				
		A	B	C	D	E
Same frequencies	σ (10^{-5}m)	0.46	0.86	1.70	3.39	6.62
	RAD (%)	0.054	0.054	0.053	0.052	0.052
Different frequencies	σ (10^{-5}m)	3.14	6.12	11.6	20.9	35.3
	RAD (%)	0.39	0.38	0.37	0.34	0.29

Note: Each value is an average value calculated based on 10 randomly generated surface profiles

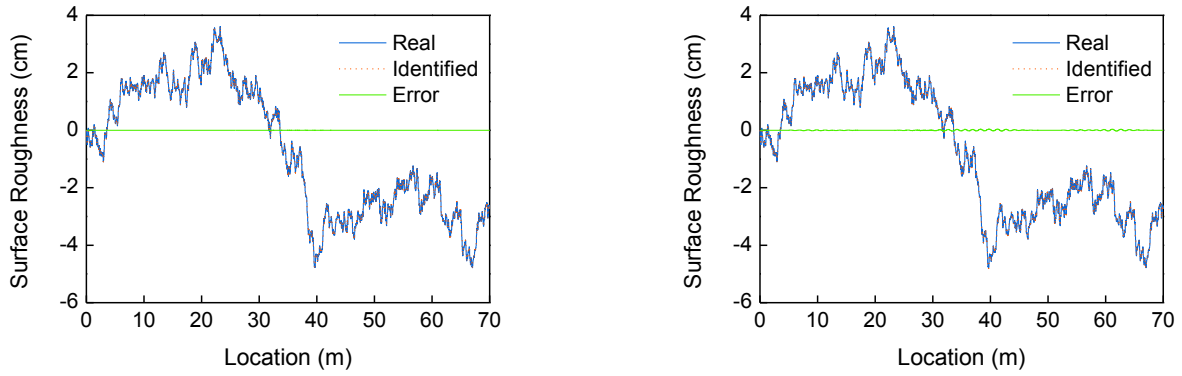

(a) Same frequency (b) Different frequency

Fig. 6 Detection results for a Class C surface profile

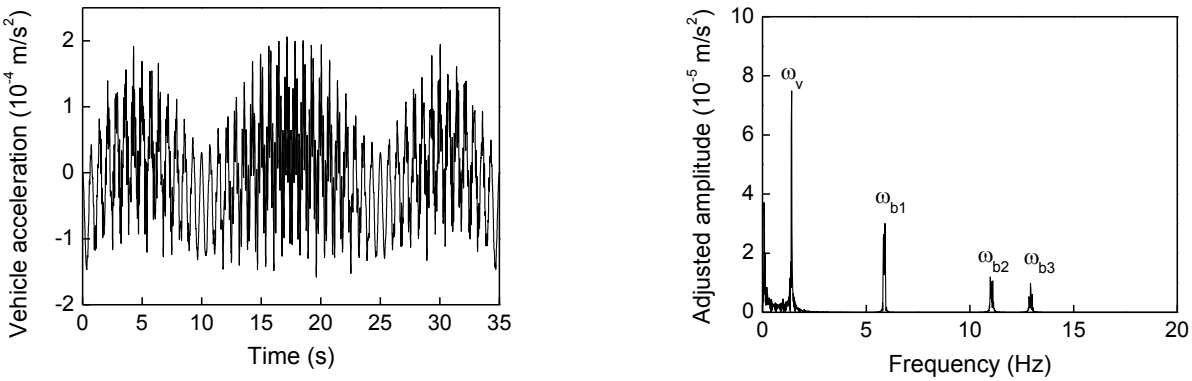

(a) Vehicle acceleration (b) Frequency spectrum

Fig. 7 Vehicle acceleration and its spectrum under smooth surface condition

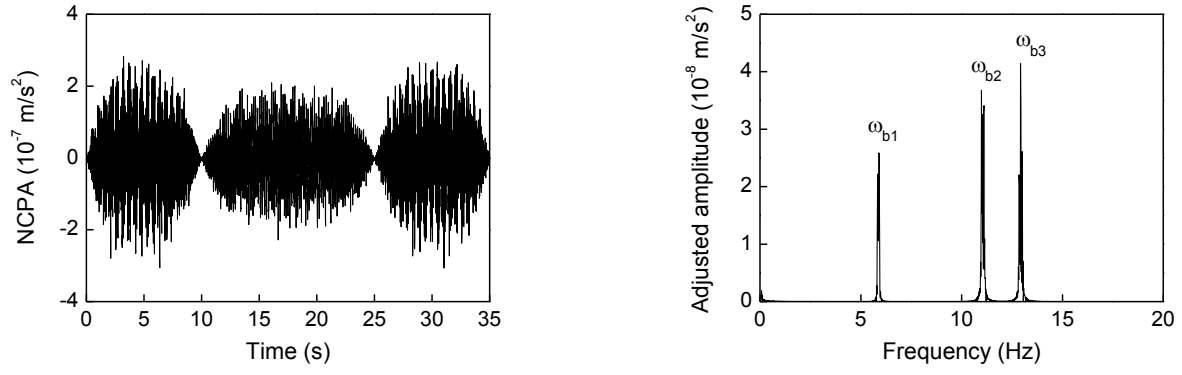

(a) NCPA (b) Frequency spectrum

Fig. 8 NCPA and its spectrum under smooth surface condition

The vehicle acceleration history presented here is that from the vehicle with mass of 2000 kg and stiffness of 154755 N×m^{-1}, and the NCPA history is that from the case f different frequencies. The frequency spectra are obtained by fast Fourier transform (FFT) from the respective time histories. For the case with smooth surface condition, the vehicle acceleration and its spectrum are presented in Fig. 7, while the NCPA and its spectrum are presented in Fig. 8. Similarly, for the case with Class C surface, the vehicle acceleration and its spectrum are presented in Fig. 9, while the NCPA and its spectrum are presented in Fig. 10. Similar results can be obtained under other classes of surface roughness, which are not shown here for conciseness.

Comparing Figs. 7 and 8, one can find that when the surface is smooth, the bridge frequencies can be easily identified by peaks in the frequency spectra of both the vehicle acceleration and NCPA. The vehicle acceleration spectrum contains vehicle frequency (Yang and Lin 2005) while the NCPA spectrum does not, which is shown in Eq. (18).

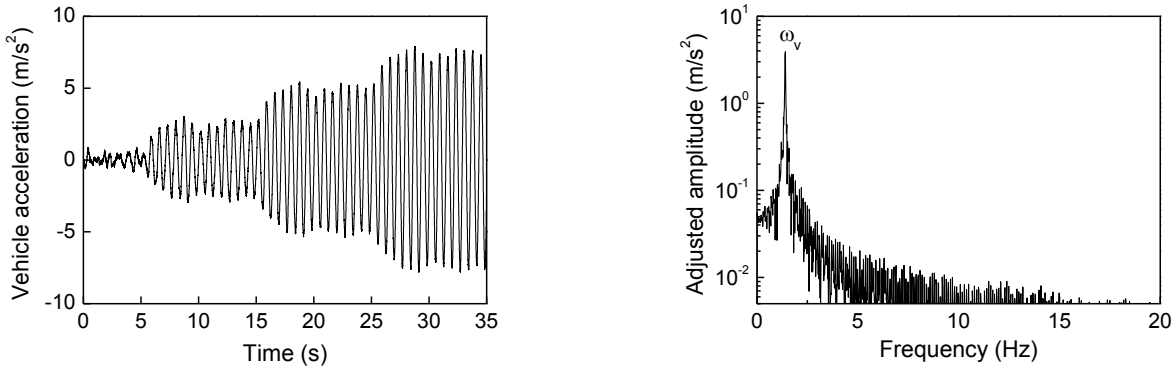

(a) Vehicle acceleration (b) Frequency spectrum

Fig. 9 Vehicle acceleration and its spectrum under Class C surface condition

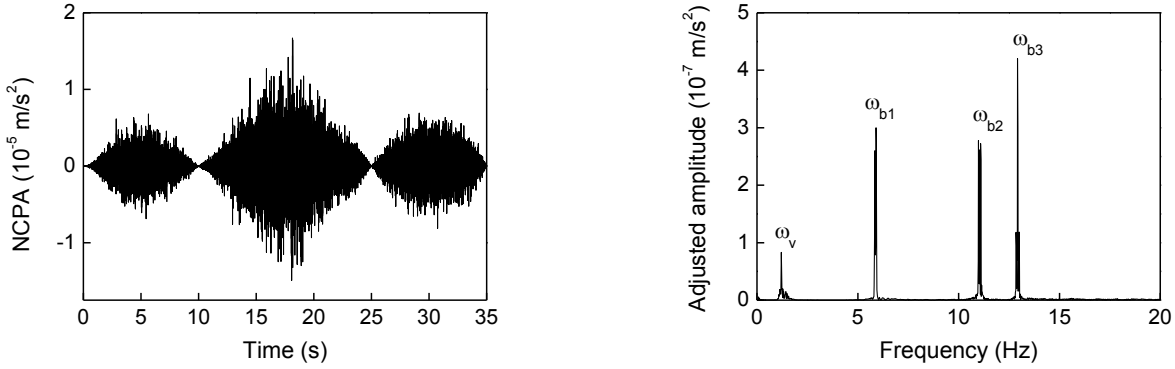

(a) NCPA (b) Frequency spectrum

Fig. 10 NCPA and its spectrum under Class C surface condition

The first three bridge frequencies obtained from theoretical analysis are 5.87, 11.06 and 12.96 Hz, respectively. The frequencies identified from the NCPA frequency spectrum are 5.89, 11.06, and 12.92 Hz, which can be considered accurate in view of the resolution of FFT of 0.0153 Hz. Now that the bridge frequencies are identified, it is convenient to extract the component accelerations related to these frequencies from the NCPA using a proper band-pass filter. However, once the surface roughness is considered, the frequency spectrum of vehicle acceleration as shown in Fig. 9 is contaminated severely and none of the bridge frequencies is identifiable. The frequency spectrum is plotted to logarithmic scale for clarity. Component acceleration extraction is therefore impossible. However, the NCPA is much less influenced by the surface roughness, and its spectrum has clear peaks that match the bridge frequencies as shown in Fig. 10. Comparing Fig. 8(b) with Fig. 10(b), one can find that the NCPA is largely immune to surface roughness contamination with only some residual effect left such as the peak corresponding to the vehicle frequency ω_v and some noise of small magnitude.

The component acceleration associated with the first three bridge frequencies obtained from the NCPA using band-pass filter under Class C surface condition are displayed in Fig. 11. Performing Hilbert transform on the component acceleration to get the envelope, adjusting the sign and normalizing, one can get the mode shapes of the bridge. The mode shapes obtained by Hilbert transform and the theoretical ones are compared in Fig. 12. One can find that the mode shapes identified match well with the theoretical ones with only some deviation near the ends.

To evaluate the performance of mode shape extraction, MAC is adopted. The MACs of the mode shapes obtained under different surface conditions are presented in Table 3. One can observe that all the MACs are higher than or close to 0.99, indicating a high identification accuracy of the proposed method. The MACs of the lowest three mode shapes of a simply supported beam extracted from the vehicle acceleration responses with smooth surface are 0.9984, 0.9999 and 0.9981, respectively (Yang *et al*. 2014). Therefore, it can be concluded that, using the NCPA obtained by the 2P2V method, one can achieve similar accuracy in the presence of surface roughness as compared to those obtained from the use of vehicle acceleration without surface roughness. In addition, unlike the estimation of surface profiles, the extraction of mode shapes is insensitive to the frequency difference between the test vehicles, which makes sense as the extraction of mode shape only requires a portion filtered out from the response. As long as this portion is unaffected, the discrepancy caused by the frequency difference will not be reflected in the extracted mode shapes.

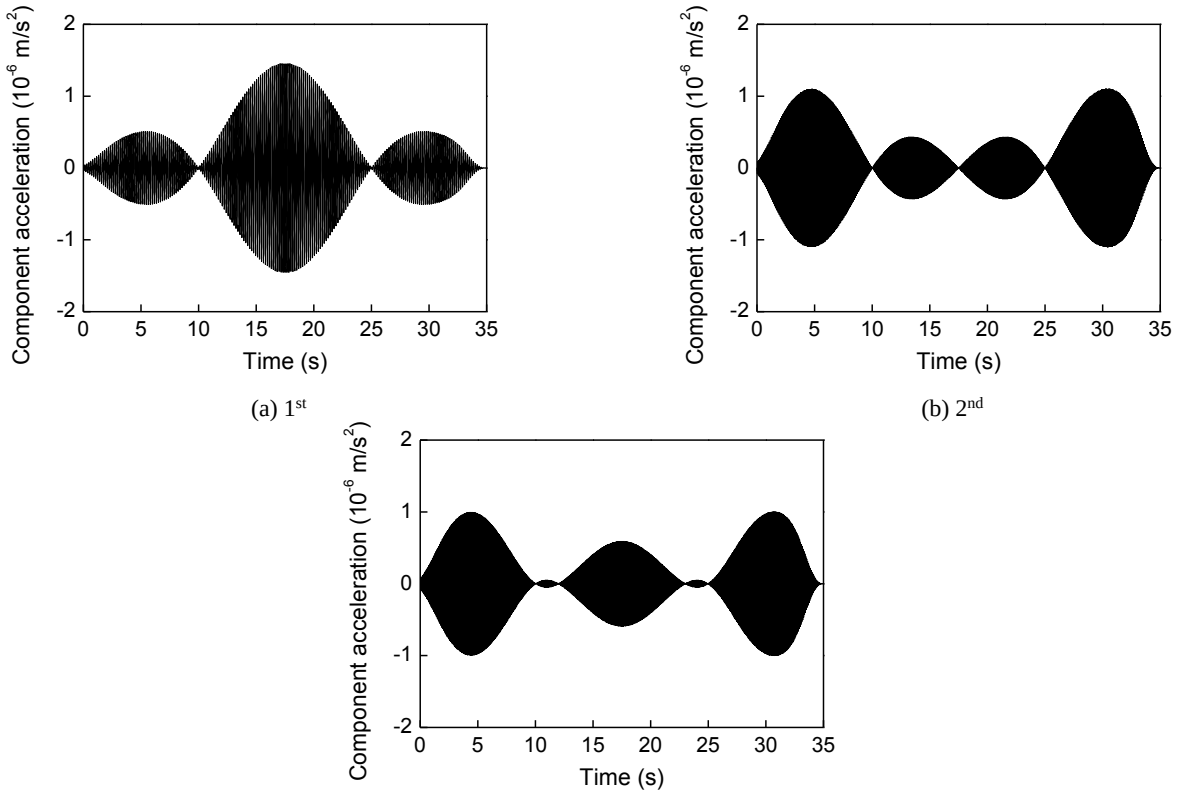

(a) 1st (b) 2nd

(c) 3rd

Fig. 11 Component acceleration extracted from NCPA under Class C surface roughness

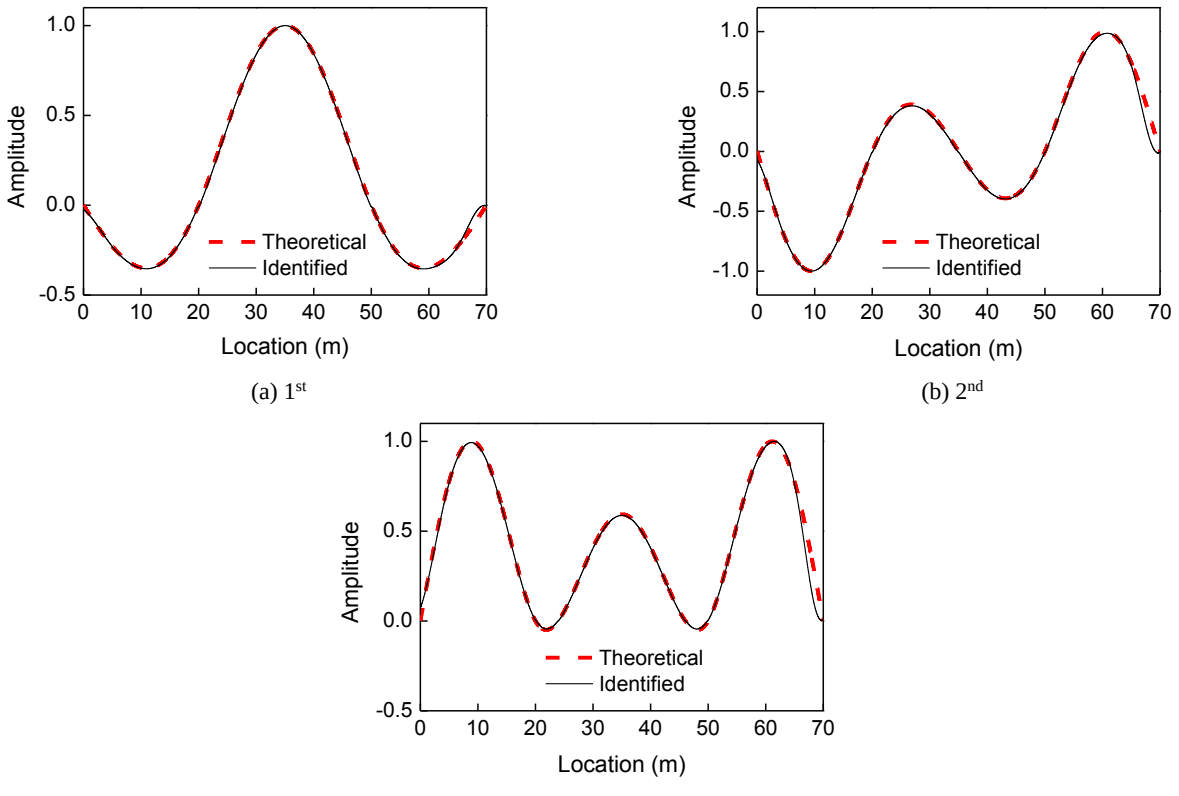

(a) 1st (b) 2nd

(c) 3rd

Fig. 12 Mode shapes obtained from component acceleration under Class C surface roughness

Table 3 MAC of the extracted mode shapes under different surface condition

Case	Mode shape	Surface roughness classes					
		Smooth	A	B	C	D	E
Same frequencies	1st	0.9991	0.9992	0.9991	0.9989	0.9991	0.9974
	2nd	0.9980	0.9984	0.9981	0.9977	0.9969	0.9943
	3rd	0.9981	0.9979	0. 9973	0.9966	0.9927	0.9913
Different frequencies	1st	0.9997	0.9997	0.9995	0.9990	0.9983	0.9967
	2nd	0.9978	0.9982	0.9971	0.9966	0.9951	0.9932
	3rd	0.9980	0.9984	0.9975	0.9962	0.9932	0.9897

Note: Each value is an average value calculated based on 10 randomly generated surface profiles except for the case of smooth surface

Table 4 Range of MACs of the extracted mode shapes for Class C surface roughness with measurement noise

Mode shape	Noise-to-signal ratio $= \frac{P_{noise}}{P_{signal}} = \frac{A_{noise}^2}{A_{signal}^2}$ P: power of signal; A: amplitude of signal		
	1%	2%	5%
1st	0.9926 ~ 0.9946	0.9901 ~ 0.9942	0.9894 ~ 0.9941
2nd	0.9897 ~ 0.9933	0.9890 ~ 0.9911	0.9807 ~ 0.9910
3rd	0.9939 ~ 0.9961	0.9926 ~ 0.9959	0.9890 ~ 0.9942

Note: The range is taken as the minimum and maximum MACs calculated from 10 cases with random noise

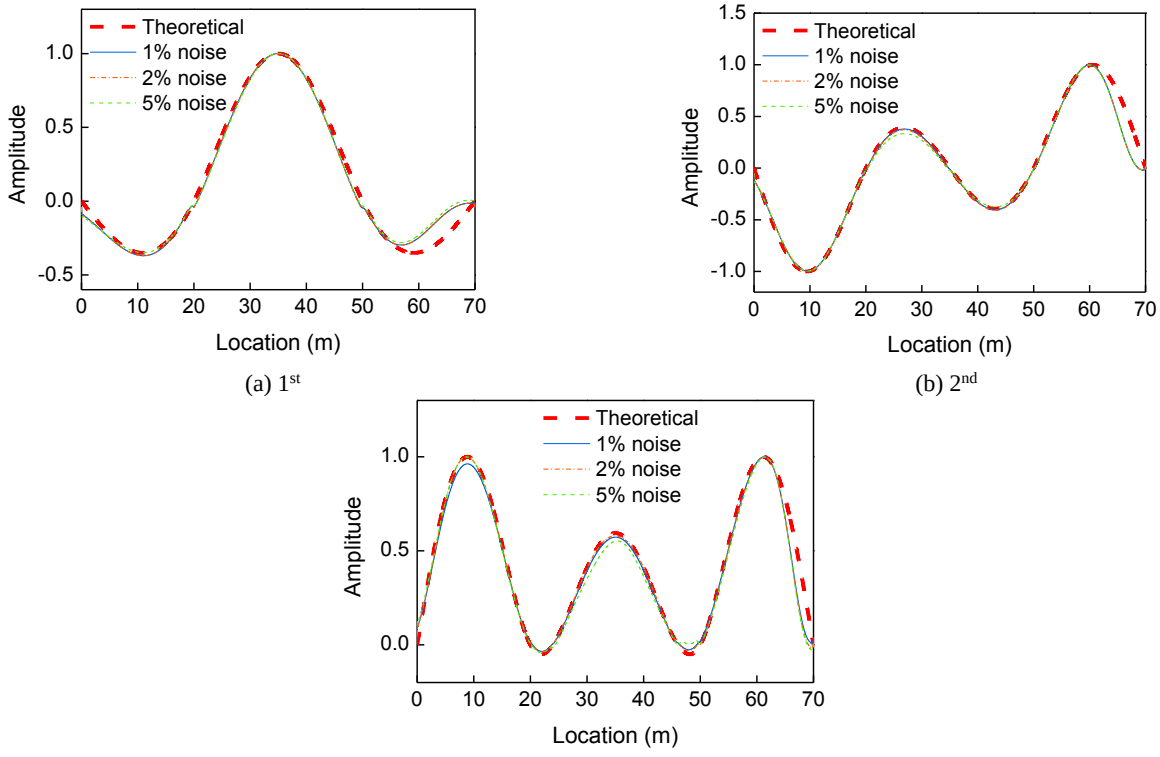

(a) 1st (b) 2nd

(c) 3rd

Fig. 13 Mode shapes extracted from NCPA with measurement noise

4.4 Influence of measurement noise

The influence of measurement noise is investigated by adding 1%, 2% and 5% of white Gaussian noise to the measured acceleration histories of the two passes. The ranges of MAC based on 10 simulations with random noise under the condition of a Class C surface roughness profile using two vehicles with different frequencies are presented

in Table 4. Some results of mode shapes are shown in Fig. 13. One can find that the method is not too sensitive to measurement noise in respect of mode shape construction. The effect of measurement noise on the surface roughness profile identified is however much more significant, and possible ways to mitigate such adverse effects have been discussed by Zhan and Au (2019).

5. Conclusions

Bridge parameter identification using the data collected from passing-by vehicle is a promising method with the advantages of economy and convenience. However, the application is often restricted due to its vulnerability to environmental noise. One of the biggest challenges is that the vehicle response is severely affected by the bridge surface roughness, and therefore it is difficult to identify the bridge information solely based on vehicle responses in the presence of surface roughness. This paper proposes a method to estimate the surface roughness profile and identify the bridge frequencies and mode shapes. First, the equations and solutions of vehicle-bridge interaction dynamics considering surface roughness are presented. Then the method of 2P2V technique to identify the surface roughness is proposed together with a discussion of its solution. Once the NCPA is obtained, the bridge frequencies and mode shapes can be identified accordingly using FFT and Hilbert transform. Two sets of numerical examples, with the same and different vehicle frequencies, are presented. A study of the vehicle response and normalized contact point response is conducted to examine their different behaviour in the presence of surface roughness.

The following conclusions are drawn: (a) The 2P2V method can estimate the surface profile with satisfactory accuracy for all 5 classes of surface quality with no requirement of prior information about the bridge; (b) The frequencies and mode shapes can be extracted from the NCPA, which is less influenced by the surface roughness compared to the vehicle acceleration; and (c) The estimation of surface roughness profile is sensitive to the frequency difference between the two test vehicles, but the extraction of mode shapes is not.

Acknowledgments

The first author is financially supported by the Hong Kong PhD Fellowship offered by the Research Grants Council of Hong Kong, which is gratefully acknowledged.

References

Altunisik, A.C., Bayraktar, A. and Ozdemir, H. (2012), "Seismic safety assessment of eynel highway steel bridge using ambient vibration measurements", *Smart Struct. Syst., Int. J.*, **10**(2), 131-154. https://doi.org/10.12989/sss.2012.10.2.131

Brownjohn, J.M.W., Xia, P.Q., Hao, H. and Xia, Y. (2001), "Civil structure condition assessment by FE model updating: methodology and case studies", *Finite. Elem. Anal. Des.*, **37**(10), 761-775. https://doi.org/10.1016/S0168-874X(00)00071-8

Bu, J.Q., Law, S.S. and Zhu, X.Q. (2006), "Innovative bridge condition assessment from dynamic response of a passing vehicle", *J. Eng. Mech.*, **132**(12), 1372-1379. https://doi.org/10.1061/(ASCE)0733-9399(2006)132:12(1372)

Camara, A., Nguyen, K., Ruiz-Teran, A. and Stafford, P. (2014), "Serviceability limit state of vibrations in under-deck cable-stayed bridges accounting for vehicle-structure interaction", *Eng. Struct.*, **61**, 61-72. https://doi.org/10.1016/j.engstruct.2013.12.030

Captain, K.M., Boghani, A.B. and Wormley, D.N. (1979), "Analytical tire models for dynamic vehicle simulation", *Vehicle Syst. Dyn.*, **8**(1), 1-32. https://doi.org/10.1080/00423117908968566

Chang, K.C., Wu, F.B. and Yang, Y.B. (2011), "Disk model for wheels moving over highway bridges with rough surfaces", *J. Sound Vib.*, **330**(20), 4930-4944. https://doi.org/10.1016/j.jsv.2011.05.002

Cheng, Y.S., Au, F.T.K., Cheung, Y.K. and Zheng, D.Y. (1999), "On the separation between moving vehicles and bridge", *J. Sound Vib.*, **222**(5), 781-801. https://doi.org/10.1006/jsvi.1998.2134

Chrysostomou, C.Z. and Stassis, A. (2008), "Health-monitoring and system-identification of an ancient aqueduct", *Smart Struct. Syst., Int. J.*, **4**(2), 183-194. https://doi.org/10.12989/sss.2008.4.2.183

Clough, R.W. and Penzien, J. (2003), *Dynamics of Structures*, McGraw-Hill, New York, NY, USA.

Elhattab, A., Uddin, N. and O'Brien, E.J. (2016), "Drive-by bridge damage monitoring using Bridge Displacement Profile Difference", *J. Civil Struct. Health Monit.*, **6**(5), 839-850. https://doi.org/10.1007/s13349-016-0203-6

Gillespie, T.D. (1997), *Vehicle Dynamics*, SAE International, Warrendale, PA, USA.

González, A., O'Brien, E. and McGetrick, P. (2012), "Identification of damping in a bridge using a moving instrumented vehicle", *J. Sound Vib.*, **331**(18), 4115-4131. https://doi.org/10.1016/j.jsv.2012.04.019

He, X.W., Kawatani, M., Hayashikawa, T., Kim, C.W., Catbas, F.N. and Furuta, H. (2014), "A structural damage detection approach using train-bridge interaction analysis and soft computing methods", *Smart Struct. Syst., Int. J.*, **13**(5), 869-890. https://doi.org/10.12989/sss.2014.13.5.869

ISO (2016), Mechanical vibration-Road surface profiles-Reporting of measured data; International Organization for Standardization, Geneva, Switzerland.

Keenahan, J., O'Brien, E.J., McGetrick, P.J. and Gonzalez, A. (2014), "The use of a dynamic truck–trailer drive-by system to monitor bridge damping", *Struct. Health Monit.*, **13**(2), 143-157. https://doi.org/10.1177/1475921713513974

Kim, C.W., Isemoto, R., McGetrick, P., Kawatani, M. and O'Brien, E.J. (2014), "Drive-by bridge inspection from three different approaches", *Smart Struct. Syst., Int. J.*, **13**(5), 775-796. https://doi.org/10.12989/sss.2014.13.5.775

Li, Z.H. and Au, F.T.K. (2014), "Damage detection of a continuous bridge from response of a moving vehicle", *Shock Vib.*, 146802. https://doi.org/10.1155/2014/146802

Lin, C.W. and Yang, Y.B. (2005), "Use of a passing vehicle to scan the fundamental bridge frequencies: An experimental verification", *Eng. Struct.*, **27**(13), 1865-1878. https://doi.org/10.1016/j.engstruct.2005.06.016

Malekjafarian, A. and Obrien, E.J. (2017), "On the use of a passing vehicle for the estimation of bridge mode shapes", *J. Sound Vib.*, **397**, 77-91. https://doi.org/10.1016/j.jsv.2017.02.051

Malekjafarian, A., McGetrick, P.J. and O'Brien, E.J. (2015), "A review of indirect bridge monitoring using passing vehicles", *Shock Vib.*, 286139. https://doi.org/10.1155/2015/286139

O'Brien, E.J. and Keenahan, J. (2015), "Drive-by damage

detection in bridges using the apparent profile", *Struct. Control Hlth.*, **22**(5), 813-825. https://doi.org/10.1002/stc.1721

O'Brien, E.J., McGetrick, P. and González, A. (2014), "A drive-by inspection system via vehicle moving force identification", *Smart Struct. Syst., Int. J.*, **13**(5), 821-848. https://doi.org/10.12989/sss.2014.13.5.821

Oliva, J., Goicolea, J.M., Astiz, M.Á. and Antolín, P. (2013), "Fully three-dimensional vehicle dynamics over rough pavement", *Proc. Inst. Civil Eng. Transp.*, **166**(3), 144-157. https://doi.org/10.1680/tran.11.00006

Oshima, Y., Yamamoto, K. and Sugiura, K. (2014), "Damage assessment of a bridge based on mode shapes estimated by responses of passing vehicles", *Smart Struct. Syst., Int. J.*, **13**(5), 731-753. https://doi.org/10.12989/sss.2014.13.5.731

Qi, Z.Q. and Au, F.T.K. (2016), "Identifying Mode Shapes of Girder Bridges Using Dynamic Responses Extracted from a Moving Vehicle Under Impact Excitation", *Int. J. Struct. Stab. Dyn.*, **17**(8), 1750081. https://doi.org/10.1142/S021945541750081X

Yang, Y.B. and Chang, K.C. (2009), "Extracting the bridge frequencies indirectly from a passing vehicle: Parametric study", *Eng. Struct.*, **31**(10), 2448-2459. https://doi.org/10.1016/j.engstruct.2009.06.001

Yang, Y.B. and Lin, C.W. (2005), "Vehicle–bridge interaction dynamics and potential applications", *J. Sound Vib.*, **284**(1), 205-226. https://doi.org/10.1016/j.jsv.2004.06.032

Yang, Y.B. and Yang, J.P. (2017), "State-of-the-art review on modal identification and damage detection of bridges by moving test vehicles", *Int. J. Struct. Stab. Dyn.*, **18**(2), 1850025. https://doi.org/10.1142/S0219455418500256

Yang, Y.B., Lin, C.W. and Yau, J.D. (2004), "Extracting bridge frequencies from the dynamic response of a passing vehicle", *J. Sound Vib.*, **272**(3), 471-493. https://doi.org/10.1016/S0022-460X(03)00378-X

Yang, Y.B., Li, Y.C. and Chang, K.C. (2012), "Using two connected vehicles to measure the frequencies of bridges with rough surface: a theoretical study", *Acta Mech.*, **223**(8), 1851-1861. https://doi.org/10.1007/s00707-012-0671-7

Yang, Y.B., Li, Y.C. and Chang, K.C. (2014), "Constructing the mode shapes of a bridge from a passing vehicle: a theoretical study", *Smart Struct. Syst., Int. J.*, **13**(5), 797-819. https://doi.org/10.12989/sss.2014.13.5.797

Yang, Y.B., Zhang, B., Qian, Y. and Wu, Y. (2018), "Contact-point response for modal identification of bridges by a moving test vehicle", *Int. J. Struct. Stab. Dyn.*, **18**(5), 1850073. https://doi.org/10.1142/S0219455418500736

Yang, Y.B., Zhang, B., Chen, Y., Qian, Y. and Wu, Y. (2019), "Bridge damping identification by vehicle scanning method", *Eng. Struct.*, **183**, 637-645. https://doi.org/10.1016/j.engstruct.2019.01.041

Zhan, Y. and Au, F.T.K. (2019), "Bridge surface roughness identification based on vehicle-bridge interaction", *Int. J. Struct. Stab. Dyn.*, **19**(7), 1950069. https://doi.org/10.1142/S021945541950069X

Zhang, Y., Wang, L. and Xiang, Z. (2012), "Damage detection by mode shape squares extracted from a passing vehicle", *J. Sound Vib.*, **331**(2), 291-307. https://doi.org/10.1016/j.jsv.2011.09.004